Engineering Fracture Mechanics 86 (2012) 38–47

Contents lists available at SciVerse ScienceDirect

Engineering Fracture Mechanics

journal homepage: www.elsevier.com/locate/engfracmech

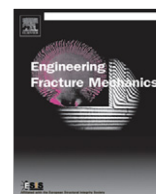

Singular stress fields at corners in flip-chip packages

Nanshu Lu [1], Zhen Zhang [2], Juil Yoon [3], Zhigang Suo *

School of Engineering and Applied Sciences, Harvard University, Cambridge, MA 02138, USA

ARTICLE INFO

Article history:
Received 12 May 2009
Received in revised form 24 January 2012
Accepted 1 February 2012

Keywords:
Flip-chip package
Corners
Split singularities
Stress intensity factors

ABSTRACT

An electronic device integrates diverse materials, and inevitably contains sharp features, such as interfaces and corners. When the device is subject to thermal and mechanical loads, the corners develop intense stress and are vulnerable sites to initiate failure. This paper analyzes stress fields at corners in flip-chip packages. The stress at a corner is a linear superposition of two modes of singular fields, with one mode being more singular than the other. The amplitudes of the two modes are represented by two stress intensity factors of dissimilar dimensions. To determine the stress intensity factors, we analyze the flip-chip structures under two loading conditions: stretching of the substrate and bending of the substrate. We show that the thermal loading of the flip-chip package is equivalent to the stretching of the substrate in generating the singular stress fields. We further show that the less singular mode may prevail over the more singular mode for some stretching-bending combinations. The relative significance of the two modes of stress fields also varies with materials, and with the substrate-to-chip thickness ratio.

© 2012 Elsevier Ltd. All rights reserved.

1. Introduction

In a flip-chip package, a silicon chip is flipped, with the face containing active devices connected to a substrate by solder bumps and underfill. The silicon chip is about 1 cm wide and 0.7 mm thick. The substrate has a width of several centimeters and a thickness of several millimeters. The material of the substrate can be either a ceramic or an organic. For example, in the mid-1990s ceramic substrates were replaced by organic laminates like FR4 (Flame Retardant 4) or BT (Bismaleimide and Triazine) resin. These organic substrates have a lower dielectric constant, have smaller thermal mismatch with the mother board, and are easier to process metallization [1]. Nevertheless, the organic substrates have several disadvantages, such as adsorption of moisture, large thermal mismatch with the silicon chip, severe warpage during assembly [2,3]. As a result, novel ceramic substrates have also been developed; for example, Low Temperature Co-fired Ceramic (LTCC), a ceramic–glass composite with elastic and thermal properties comparable to those of silicon, is a potential choice for the substrate. LTCC is fired at sufficiently low temperature so that copper can be used in the metallization. The ceramic substrate also offers superior hermetic and mechanical stability to protect the chip [4]. Table 1 lists the properties of silicon and the two materials for the substrate. All materials are idealized as isotropic linear elastic materials.

A structure like a flip-chip package contains diverse materials and sharp features such as interfaces and corners. When the structure is subject to thermal and mechanical loads, the stress field intensifies at the corners, making them vulnerable sites to initiate failure [3,5–13]. A challenge to analyze stress in flip-chip packages is the large variation in length scales, from the

* Corresponding author.
E-mail address: suo@seas.harvard.edu (Z. Suo).
[1] Present address: Department of Aerospace Engineering and Engineering Mechanics, The University of Texas at Austin, Austin, TX 78712, USA.
[2] Present address: Microsoft Corp., Silicon Valley Campus, 1065 La Avenida, Mountain View, CA 94043, USA.
[3] Present address: Department of Mechanical Systems Engineering, Hansung University, Seoul 136-792, South Korea.

0013-7944/$ - see front matter © 2012 Elsevier Ltd. All rights reserved.
http://dx.doi.org/10.1016/j.engfracmech.2012.02.010

Table 1
Material properties for chip and substrates used in calculation.

	E (GPa)	ν	*CTE* (ppm/°C)
Silicon	130	0.28	3.3
FR4	23	0.3	15
LTCC	120	0.3	5.8

chip-substrate level of several centimeters down to the smallest transistors of several nanometers. To fully capture the chip-substrate behavior, a multi-scale finite element method, known as global–local submodeling, is widely adopted [9,11,14]. Simulations of this kind, however, are tedious and expensive. Improved understandings of significant features in such structures are valuable.

This paper focuses on chip-substrate corners shown in Fig. 1a. As discussed in the next section, we will apply the concept of split singularities to analyze the stress field at the corners. While the mechanics of split singularities at corners has been studied, here we apply the approach to an engineering structure to elucidate the relative significance of the two modes of singular stress fields. The paper is organized as follows. Section 2 summarizes the concept of split singularities. Section 3 shows how to calculate the two stress intensity factors and the mode angle under combined stretching and bending of the substrate. In Section 4, we investigate the relative contributions of the two singular modes for two substrate materials: FR4 and LTCC. Section 5 studies the significance of each mode for various chip-substrate geometries. Discussions focusing on thermal loading and failure criterion are given in Section 6. Concluding remarks are provided in Section 7.

2. Split singularities

For a linearly elastic bimaterial with traction prescribed on the boundary, Dundurs [15] demonstrated that the stress field depends on elastic constants through two dimensionless parameters:

$$\alpha = \frac{E_c(1-\nu_s^2) - E_s(1-\nu_c^2)}{E_c(1-\nu_s^2) + E_s(1-\nu_c^2)}, \tag{1}$$

$$\beta = \frac{1}{2}\frac{E_c(1+\nu_s)(1-2\nu_s) - E_s(1+\nu_c)(1-2\nu_c)}{E_c(1+\nu_s)(1-2\nu_s) + E_s(1+\nu_c)(1-2\nu_c)}, \tag{2}$$

where E is Young's modulus, and ν Poisson's ratio. The subscripts "*c*" and "*s*" refer to the chip and the substrate, respectively. By requiring $E > 0$ and $0 \leqslant \nu \leqslant 0.5$, the Dundurs parameters are confined within a parallelogram in the (α, β) plane, with vertices at $(1, 0)$, $(1, 0.5)$, $(-1, 0)$ and $(-1, -0.5)$.

Fig. 1b magnifies the bimaterial corner. A system of polar coordinates (r, θ) is attached, with the origin coinciding with the intersection of the edge of the chip and the surface of the substrate. The two materials are bonded along the interface $\theta = 0°$. The chip occupies the quarter space, $0° \leqslant \theta \leqslant 90°$, and the substrate occupies the half space, $-180° \leqslant \theta \leqslant 0°$. Both the chip and the substrate are taken to be linearly elastic and isotropic. All edges and interfaces are assumed to be perfectly sharp.

We next summarize the main results of the singular stress fields around the corner [16–18]. Each component of the stress takes the form of $\sigma_{ij} \sim r^{-\lambda}$, where λ is the exponent of the singular field. This singular stress field is determined by an eigenvalue problem [16–23]. The exponent is commonly restricted in the interval $0 < \mathrm{Re}(\lambda) < 1$, with justifications critiqued by Hui and Ruina [24] and Labossiere and Dunn [25].

For many combinations of materials, two unequal and real exponents are found, which are labeled such that $\lambda_1 > \lambda_2$. This paper focuses on this case. The stress around the corner is a linear superposition of the two modes of singular fields:

$$\sigma_{ij}(r,\theta) = \frac{k_1}{(2\pi r)^{\lambda_1}}\Sigma_{ij}^1(\theta) + \frac{k_2}{(2\pi r)^{\lambda_2}}\Sigma_{ij}^2(\theta). \tag{3}$$

The angular functions, $\Sigma_{ij}^1(\theta)$ and $\Sigma_{ij}^2(\theta)$, are normalized such that $\Sigma_{r\theta}^1(0) = \Sigma_{r\theta}^2(0) = 1$, and their full expressions are listed in Appendix A. k_1 and k_2 are called the *stress intensity factors*, analogous to the stress intensity factors K_{I} and K_{II} for a crack.

The singular stress field, Eq. (3), is only valid within an annulus, as highlighted in Fig. 1b. Within the process zone, where $r < \Lambda$, there may be nonlinear behavior of materials and geometric perturbations. Material defects and interfacial flaws may also appear. On the other hand, an outer boundary for the validity of Eq. (3) also exists. Because at a length scale close to the chip thickness h, the external boundary conditions will distort the radial variance of stresses characterized by Eq. (3). Therefore as long as the process zone is significantly smaller than the macroscopic chip height, i.e. $\Lambda \ll h$, the singular stress field governed by Eq. (3) will prevail within an annulus, known as the *k*-annulus. In the following discussion we will mainly focus on the singular stress field within the *k*-annulus.

In fracture mechanics, so long as the square-root singular fields prevail in an annulus, the stress intensities, K_{I} and K_{II}, are the only parameters that link external loadings to the material response inside the process zone. Consequently, the stress intensity factors can be used to formulate critical conditions for crack extension. In the same spirit, k_1 and k_2 may be used to formulate critical conditions to initiate failure at sharp corners [24,26,27].

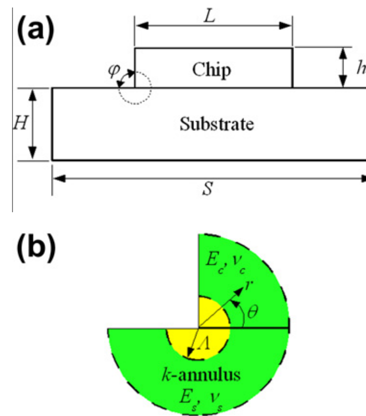

Fig. 1. (a) Simplified 2D chip-substrate model with materials listed in Table 1. Plane strain conditions are assumed. (b) Blown up chip-substrate interface corner highlighted in (a) with process zone of radius Λ and the k-annulus. A system of polar coordinates (r, θ) is defined.

Eq. (3) indicates that, in general, two singular modes, Mode 1 and Mode 2, govern the stress field in the k-annulus. For example, consider a homogeneous body with a sharp notch and an axis of symmetry. Any external loading condition can be decomposed into a symmetric mode (Mode 1) and an anti-symmetric mode (Mode 2). Mode 1 corresponds to pure tension and Mode 2 represents pure shear with respect to the symmetric axis.

For a bimaterial corner, however, no such axis of symmetry exists, so that no simple geometric interpretation of the two singular modes is available. If we fix the opening angle $\varphi = 90°$ as shown in Fig. 1b but vary the elastic constants of the two materials, the singular exponents will change accordingly. Solving the eigenvalue problem, we plot λ_1 and λ_2 as functions of the Dundurs parameter, α, in Fig. 2, with β fixed to be zero. The plot shows that, while λ_1 is always close to 0.5, λ_2 varies substantially with the elastic mismatch. When $\alpha \to -1$ i.e. $E_c/E_s \to 0$, λ_2 goes to zero. When $\alpha \to 1$, namely $E_c/E_s \to \infty$, λ_2 approaches 0.5. Indicated in Fig. 2 are the singular components for two combinations of materials: Si/LTCC and Si/FR4.

When $\lambda_1 \neq \lambda_2$, according to Eq. (3), k_1 and k_2 have different dimensions, $(\text{stress})(\text{lengh})^{\lambda_1}$ and $(\text{stress})(\text{lengh})^{\lambda_2}$, respectively. Hence the ratio of Mode 2 to Mode 1 stress can be written as $(k_2/k_1)r^{\lambda_1-\lambda_2}$, where r can be an arbitrary length [18]. Labossiere et al. [28] have used this mode mixity in describing their experimental data. A similar approach was taken to describe the split singularities around a bimaterial interfacial crack tip [29].

To quantify the mode mixity we fix the arbitrary length scale to be the process zone size Λ. Thus, a *mode angle*, ψ, is defined as

$$\tan\psi = \frac{k_2}{k_1}\Lambda^{\lambda_1-\lambda_2}. \tag{4}$$

When the stress state at $r = \Lambda$ is pure Mode 1, $\psi = 0°$; when it is pure Mode 2, $\psi = 90°$.

Mode 2 has often been neglected due to the fact that the Mode 2 stress field is always less singular than Mode 1, as indicated in Fig. 2 [6,30,31]. Moreover, it is much simpler to use one stress intensity factor to implement a fracture initiation

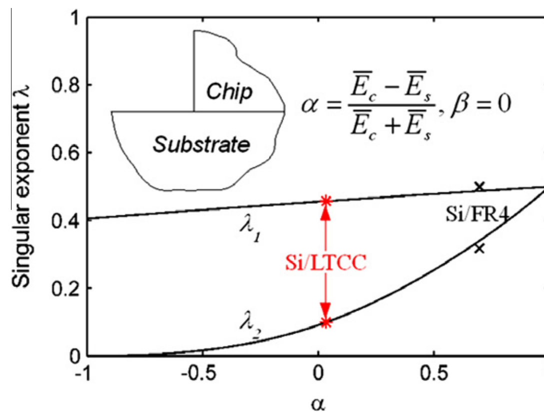

Fig. 2. Split singularities at orthogonal interface corner as functions of elastic mismatch, denoted by Dundurs parameter α, with β fixed to be zero. Stars highlight the singular exponents when Chip = Si and Substrate = LTCC. Crosses show the singular exponents for Chip = Si and Substrate = FR4. Since β is not exactly zero in this case, the points are slightly off the curves.

criterion at the bimaterial interface corner. However, whether Mode 2 is negligible or not depends on its relative significance compared to Mode 1, which is captured by the mode angle. In the following, we will calculate the mode angles for chip-substrate systems with different substrate materials or geometries under various loading conditions. Our results provide insights into situations when Mode 2 can be significant.

3. Calculation of stress intensity factors

The two stress intensity factors k_1 and k_2 are determined by solving boundary-value problems. As depicted in Fig. 3, we will solve boundary value problems under two loading conditions: stretching of the substrate and bending of the substrate. During processing, the substrate is also subject to a change in temperature, leading to stress concentration around chip-substrate corners (Fig. 4). As shown in Appendix B, the change in temperature and the stretching stress are linearly dependent loading conditions and can give rise to the same stress intensity factors at the corner, provided the stretching stress is identified as

$$p = \bar{E}_s[(1+\nu_s)\alpha_s - (1+\nu_c)\alpha_c]\Delta T, \tag{5}$$

where α_c and α_s are the respective coefficients of thermal expansion, $\bar{E}_s = E_s/(1-\nu_s^2)$ is the plane strain modulus of the substrate and ΔT the change in temperature. Therefore, even though we adopt stretching of the substrate and bending of the substrate as the loading conditions in the following analysis, thermal loading and stretching of the substrate are indeed two equivalent loading conditions.

Let P be the stretching force, and M be the bending moment per unit thickness. Dimensional analysis dictates that the stress intensity factors, k_1 and k_2, relate to the loading parameters, P and M, through

$$\frac{k_1}{h^{\lambda_1}} = b_{11}\cdot\frac{P}{h} + b_{12}\cdot\frac{M}{h^2}, \tag{6}$$

$$\frac{k_2}{h^{\lambda_2}} = b_{21}\cdot\frac{P}{h} + b_{22}\cdot\frac{M}{h^2}. \tag{7}$$

Because the boundary-value problems are linear, the b coefficients are independent of the loading parameters, but depend on material properties and various dimensionless ratios, including E_c/E_s, H/h, L/h, and S/h.

We solve the two boundary-value problems by using the commercial finite element method (FEM) code ABAQUS 6.7. Plane strain conditions are assumed. For each boundary value problem, the stress field along $\theta = 0°$ as a function of r, for

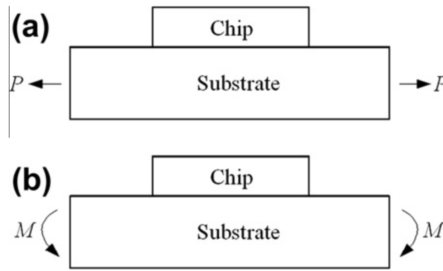

Fig. 3. Two linearly independent loading conditions: (a) stretching force P applied on the substrate; (b) bending moment M applied on the substrate.

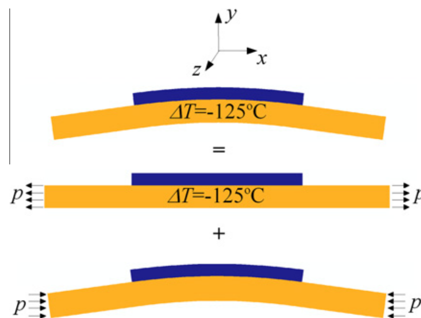

Fig. 4. Equivalent singular stress fields around chip-substrate corners can be generated by either thermal loading ΔT on the chip-substrate system or uniform uniaxial tension $p = \bar{E}_s\Delta T[(1+\nu_c)\alpha_c - (1+\nu_s)\alpha_s]$ on the substrate, as derived in Appendix B. All pictures are directly output from ABAQUS.

example $\tau_{r\theta}(r, \theta = 0)$, can be extracted from the FEM results. To make sure it falls in the k-annulus, we take $10^{-3} < r/h < 10^{-2}$. According to Eq. (3) and the way we normalize the angular functions, the stress field along the interface is given by

$$\tau_{r\theta}(r,\theta=0)=\frac{k_1}{(2\pi r)^{\lambda_1}}+\frac{k_2}{(2\pi r)^{\lambda_2}}. \tag{8}$$

The two stress intensity factors are determined by using least square fitting of the stress $\tau_{r\theta}(r, \theta = 0)$ calculated from the FEM to Eq. (8). The boundary-value problem of stretching ($P = 1, M = 0$) determines the coefficients b_{11} and b_{21}. The boundary-value problem of bending ($P = 0, M = 1$) determines the coefficients b_{12} and b_{22}.

Once the b coefficients are determined, Eqs. (6) and (7) can be used to calculate the stress intensity factors under any combined loads of stretching, bending and change in temperature. Substituting Eqs. (6) and (7) into Eq. (4), we find that the mode angle ψ is given by

$$\tan\psi=\frac{b_{21}+b_{22}\cdot\frac{M}{Ph}}{b_{11}+b_{12}\cdot\frac{M}{Ph}}\left(\frac{\Lambda}{h}\right)^{\lambda_1-\lambda_2}. \tag{9}$$

This equation relates the mode angle to the loading parameters P and M. We will use this method to investigate the effects of substrate material and chip-substrate geometry on the relative significance of the two singular modes in the following sections.

The process zone size is set to be $\Lambda/h = 10^{-3}$ in all the following calculations. Since $0 < \Lambda/h \ll 1$ and $\lambda_1 - \lambda_2 > 0$, a larger value of Λ/h yields a larger value of $(\Lambda/h)^{\lambda_1-\lambda_2}$, and hence a larger absolute value of ψ. However, so long as we keep a consistent choice of the process zone size, the trends discussed below are valid.

4. Effect of the substrate material

A simplified 2D chip-substrate structure is sketched in Fig. 1a. The chip is of Si, and the substrate can be of either FR4 or LTCC. The Dundurs parameter for Si/FR4 and Si/LTCC systems are $\alpha \approx 0.70$ (large elastic mismatch) and $\alpha \approx 0.03$ (small elastic mismatch), respectively. The singular exponents of the two systems are also provided in Table 2 and highlighted in Fig. 2.

In all of our simulations, we fix the chip thickness $h = 0.7$ mm and normalize all other length scales by h. In this case we fix the chip-substrate geometry at $H/h = 2$, $L/h = 14.29$, and $S/h = 28.57$. Fig. 5 plots the mode angle ψ as a function of the dimensionless ratio of the loading parameters, $M/(Ph)$. Both structures, Si/FR4 and Si/LTCC, are considered. The general trends are noted below.

(a) Mode 2 ($\psi = 90°$) dominates at a small absolute value of $M/(Ph)$, where stretching prevails over bending.
(b) Mode 1 ($\psi = 0°$) dominates at a large absolute value of $M/(Ph)$, where bending prevails over stretching.
(c) Under most loading conditions, the larger elastic mismatch between the chip and the substrate, e.g. Si/FR4, yields a larger Mode 2 component.

To understand these trends, we examine Eq. (9). Observe that $\psi = 90°$ when $M/(Ph) = -b_{11}/b_{12}$. This is the point where $k_1 = 0$ according to Eq. (6). Referring to the b coefficients listed in Table 2 we note that $-b_{11}/b_{12} = -0.1478$ for Si/FR4 and $-b_{11}/b_{12} = -0.2384$ for Si/LTCC. Consequently, within a narrow band of $M/(Ph)$ where pure stretching (or thermal loading) is dominant, Mode 2 can prevail over Mode 1. Since thermal loading is the most common loading condition during the manufacture of flip-chip packages, Mode 2 contribution to the singular stress fields deserves strong emphasis.

When the external loading is bending dominant, i.e. $|M| \gg |Ph|$, Eq. (9) shows that the mode angle ψ approaches a constant

$$\psi=\tan^{-1}\left[\frac{b_{22}}{b_{12}}\left(\frac{\Lambda}{h}\right)^{\lambda_1-\lambda_2}\right], \tag{10}$$

which is calculated to be 1.49° for Si/FR4 and 1.36° for Si/LTCC. Therefore we conclude that when the chip-substrate is under pure bending or bending overwhelms stretching, the singular stress field is almost pure Mode 1.

The major difference between the two curves is the decay rate of the mode angle, from 90° to almost 0°. If we take $|\psi| > 45°$ to be the criterion for Mode 2 dominance, substitute Eq. (9) in and solve the inequality we can determine the range of $M/(Ph)$ for Mode 2 to be overwhelming:

Table 2
Dunders parameters, singular exponents and b coefficients for two chip-package systems with fixed geometry: $h = 0.7$ mm, $H/h = 2$, $L/h = 14.29$, and $S/h = 28.57$, as shown in Fig. 1a.

	α	β	λ_1	λ_2	b_{11}	b_{12}	b_{21}	b_{22}
Si/FR4	0.6961	0.1959	0.4990	0.3178	0.1117	0.7560	0.1785	0.0689
Si/LTCC	0.0337	0	0.4571	0.0996	0.1049	0.4401	0.0617	0.1238

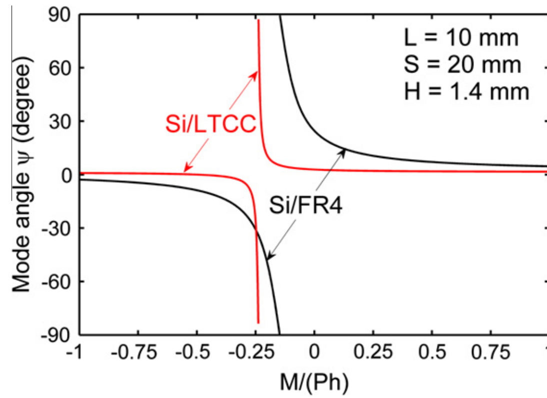

Fig. 5. Mode angle as a function of the proportion of bending to stretching for two different substrate materials: FR4 and LTCC.

$$-\frac{b_{11}+(\frac{A}{h})^{\lambda_1-\lambda_2}b_{21}}{(\frac{A}{h})^{\lambda_1-\lambda_2}b_{22}+b_{12}}<\frac{M}{Ph}<\frac{b_{11}-(\frac{A}{h})^{\lambda_1-\lambda_2}b_{21}}{(\frac{A}{h})^{\lambda_1-\lambda_2}b_{22}-b_{12}}. \qquad (11)$$

Using the values of λ and b listed in Table 2, we find that when $-0.244 < M/(Ph) < -0.232$, $|\psi| > 45°$ for Si/LTCC. For Si/FR4, the band for $|\psi| > 45°$ widens to be $-0.210 < M/(Ph) < -0.082$. This observation indicates that the larger the elastic mismatch between chip and substrate, the bigger range of $M/(Ph)$ for Mode 2 component to be significant.

In summary, Fig. 5 illustrates the relative contribution of the two singular modes at arbitrary combinations of $M/(Ph)$ for two substrate materials, FR4 and LTCC. In both cases, when $M/(Ph)$ approaches $-b_{11}/b_{12}$ from either side, the mode angle ψ increases drastically until pure Mode 2 is reached. When $M/(Ph)$ remains far from $-b_{11}/b_{12}$, the mode angle ψ stays close to 0° which means the singular stress field is Mode 1 dominant. A significant difference between the two substrate materials lies in the decay rate of the mode angle: when the substrate material is FR4, i.e. when there is a large elastic mismatch between chip and substrate, ψ decays slowly from 90° to close to 0°. As a result, Mode 2 remains significant over a bigger range of $M/(Ph)$.

5. Geometric effects

The geometry of the chip-substrate structure can also play an important role in determining the behavior of the singular stress field. We first vary the length of the chip, L/h, from 8.57 to 28.57, while keeping the other lengths fixed at $H/h = 2$, and $S/h = 57.14$. The b coefficients for different lengths of the chip remain unchanged. This conclusion recovers a previous result [32]: the stress intensity factor reaches a plateau when L/h is greater than 10. That is, when the length of the chip exceeds several times the thickness of the chip, the stress field near one edge of the chip can no longer be affected by the presence of the other edge. Therefore, further increase in L cannot alter the singular stress field at the chip-substrate corner.

We study the effect of the size of the substrate by fixing $L/h = 14.29$, and $H/h = 2$, but varying S/h from 21.43 to 85.71. The b coefficients also remain constants when S changes. That is, as long as the substrate is wide enough compared to the chip, regardless of how much further S increases, the same boundary conditions on the two edges of the substrate will result in the same local stress field around the chip-substrate corner.

By contrast, the substrate thickness H, significantly affects the behavior of the singular stress field. Table 3 and Fig. 6 show the b coefficients as functions of H/h. When H/h is large, b_{12} and b_{22} approach zero, indicating bending moment on the edges of the substrate can no longer cause noticeable singular stress around the chip-package corner; b_{11} and b_{21} approach some small but finite values, indicating stretching can still make very limited contribution to both singular modes. Compared to b_{11}, b_{12} is more sensitive to the change of the substrate thickness. Compared to b_{11} and b_{21}, b_{12} and b_{22} decay to zero from much greater values, implying that the contribution from bending is much more sensitive to the change of the substrate thickness.

Table 3
b coefficients for Si/FR4 chip-package system with various substrate thicknesses, where $h = 0.7$ mm, $L/h = 14.29$, and $S/h = 28.57$ are fixed.

H/h	b_{11}	b_{12}	b_{21}	b_{22}	$-b_{11}/b_{12}$
1/3	−0.0193	13.6450	1.2091	−4.2503	0.0014
1/2	0.0077	6.9809	0.8595	−1.2846	−0.0011
1	0.0710	2.3352	0.4234	−0.1236	−0.0304
2	0.1117	0.7560	0.1785	0.0689	−0.1478
4	0.1085	0.2396	0.0784	0.0524	−0.4529

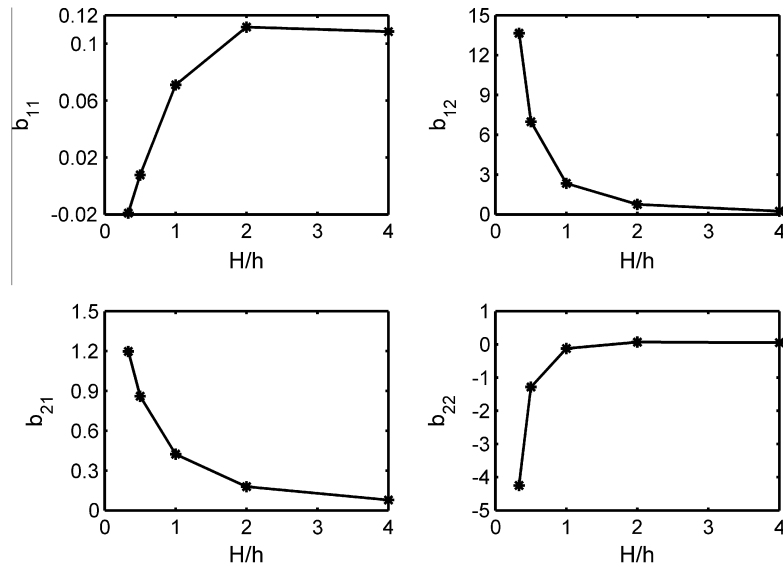

Fig. 6. *b* coefficients as functions of substrate-to-chip thickness ratio with fixed sizes of chip and substrate, $L = 10$ mm and $S = 20$ mm respectively.

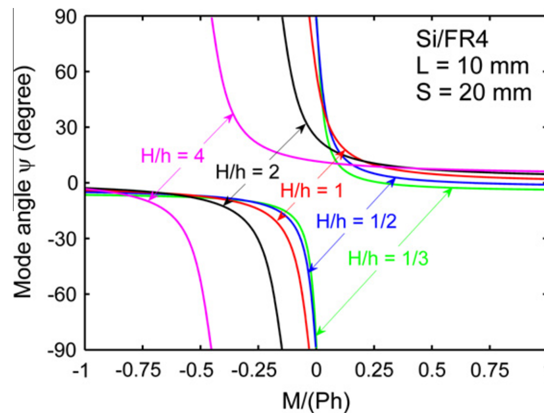

Fig. 7. Mode angle as a function of the proportion of bending to stretching for Si/FR4 chip-substrate system with various substrate-to-chip thickness ratios.

If we substitute the b coefficients listed in Table 3 into Eq. (9), a plot of mode angle ψ as a function of $M/(Ph)$ can be obtained as shown in Fig. 7. As we discussed before, ψ approaches 90° as $M/(Ph)$ goes to $-b_{11}/b_{12}$, which is also listed in Table 3. Since b_{11} remains close to zero but b_{12} rises quickly as the substrate thickness decreases, the value of $-b_{11}/b_{12}$ shifts gradually from -0.4529 to almost 0 as the substrate gets thinner. When $M/(Ph)$ is large, the value of ψ increases slightly as the substrate gets thicker. The decay rate of the mode angle with respect to $M/(Ph)$ is also affected by the substrate thickness: the thicker the substrate, the wider band of $M/(Ph)$ where Mode 2 is significant.

6. Discussions

6.1. Thermal loading

Thermal excursion is the most common loading suffered by the flip-chip packages and hence deserves some specific emphasis. In Appendix B we show that the singular stress field generated by thermal loading can be completely counteracted by simply stretching the substrate. Therefore, the stretching of the substrate can generate the same singular stress field at the chip-substrate interface corner as the thermal loading provided the tensile stress is related to the change in temperature through Eq. (5). Eq. (5) shows that p and ΔT are linearly related and they can completely represent one another. Therefore all the discussions in this paper mentioning stretching of the substrate can be interpreted for thermal loading.

When the flip-chip package is subjected to pure thermal loading, i.e. when $M/(Ph) = 0$, Figs. 5 and 7 suggest that Mode 2 can have a strong contribution in the Si/FR4 system with small substrate thickness. Under a given thermal loading, there are

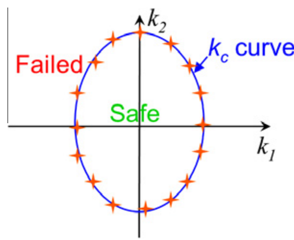

Fig. 8. Proposed fracture initiation criterion based on a critical k curve to be obtained experimentally. When (k_1, k_2) calculated by Eqs. (6) and (7) lies inside the k_c curve, the structure is safe, otherwise failure will initiate from the chip-substrate corner.

two ways to reduce the singular stress field, i.e. to decrease b_{11} and b_{21}, as given in Tables 2 and 3: to decrease the elastic mismatch between the chip and the substrate or to increase the substrate thickness.

6.2. Failure initiation criterion for mix mode singularities

When the stress field around a bimaterial interface corner is Mode 1 dominant, there is a widely established fracture initiation criterion based on a single parameter, the critical Mode 1 stress intensity factor k_{1c} [6,29,32], which is essentially of the same role as K_{IC} in the criterion for crack propagation. However, when the singular stress field is of mixed modes, and there is no single mode always overwhelming, a fracture initiation criterion taking both modes into account is necessary [33].

Here we elaborate the implementation of this criterion step by step. First, given a structure as shown in Fig. 1a and the two corresponding materials, the b coefficients defined in Eqs. (6) and (7) can be calculated as demonstrated in Section 3. When the b coefficients are available, the fracture initiation driving forces, k_1 and k_2, can be calculated from Eqs. (6) and (7) for given P and M. By comparing the driving forces with the fracture resistance one can determine whether the structure is safe or going to initiate fracture from the corners. To find out the fracture resistance, i.e. a 2D curve of critical stress intensity factors, experimental tests must be carried out. Loadings superimposing P and M as shown in Figs. 3a and b should be applied to the structure. The critical loads (P_c, M_c) at which fracture initiates from the interface corner can be recorded and then a set of (k_{1c}, k_{2c}) can be determined using Eqs. (6) and (7). Run a series of tests with different mode angles and plot the corresponding (k_{1c}, k_{2c}) pairs as data dots on a k_1–k_2 plane as shown in Fig. 8. By doing curve fitting, a critical k_c curve can be obtained, which is known as the *fracture resistance curve*. Hence to predict whether the structure is safe or not under a specific loading combination, the driving force (k_1, k_2) calculated by Eqs. (6) and (7) can be plotted on the same k_1–k_2 plane. If the dot falls inside the k_c curve the structure will stay intact. Otherwise the structure is predicted to fail under such loadings.

7. Concluding remarks

In summary, we study singular stress field at corners in flip-chip packages, when the substrate is subject to a combination of bending and stretching. It is important to notice that the thermal loading of the chip-substrate system can be completely represented by the pure stretching of the substrate through Eq. (5). The singular stress field is a superposition of two modes, of dissimilar exponents, $\lambda_1 > \lambda_2$. We compared the contributions of the two modes to the magnitude of the stress field at a length characteristic of the process zone size, Λ. We demonstrated that Mode 2 can contribute significantly when $M/(Ph)$ approaches $-b_{11}/b_{12}$. When the loading is bending dominant, however, the Mode 2 component is always very small. At most loading conditions, Mode 2 component is more significant in a chip-substrate system with larger elastic mismatch. While the lengths of the chip and the substrate have little effects on the singular stress field, the substrate-to-chip thickness ratio has a great influence. Thicker substrate shows larger range of $M/(Ph)$ for Mode 2 to dominate over Mode 1.

Acknowledgments

The work presented in this paper was supported by the National Science Foundation (NSF) under Grant CMS-0556169, and by the Materials Research Science and Engineering Center (MRSEC) at Harvard University. Juil Yoon thanks the support from the Hansung University in the year of 2009.

Appendix A. Stress components in polar coordinates

The singular stress field Eq. (3) is solved by the methods outlined in Ref. [10,5]. The eigenfunctions $\Sigma_{ij}(\theta)$ associated with the eigenvalue λ are expressed in polar coordinates (r, θ) as

$$\Sigma_{rr}(\theta) = -(\lambda - 1)\{(\lambda - 2)[A\sin(\lambda - 2)\theta + B\cos(\lambda - 2)\theta] + (\lambda + 2)[C\sin\lambda\theta + D\cos\lambda\theta]\}, \tag{A1}$$

$$\Sigma_{\theta\theta}(\theta) = (\lambda-1)(\lambda-2)[A\sin(\lambda-2)\theta + B\cos(\lambda-2)\theta + C\sin\lambda\theta + D\cos\lambda\theta], \tag{A2}$$

$$\Sigma_{r\theta}(\theta) = (\lambda-1)\{(\lambda-2)[A\cos(\lambda-2)\theta - B\sin(\lambda-2)\theta] + \lambda[C\cos\lambda\theta - D\sin\lambda\theta]\}, \tag{A3}$$

$$\Sigma_{zz}(\theta) = -4v(\lambda-1)[C\sin\lambda\theta + D\cos\lambda\theta], \tag{A4}$$

$$\Sigma_{rz} = \Sigma_{\theta z} = 0. \tag{A5}$$

The two eigenvalues λ_1 and λ_2 and the coefficients A, B, C, and D in both the chip and the substrate are determined by solving the eigenvalue problem. The values of A, B, C and D are listed in Table A1.

Appendix B. Representing thermal loading by uniform stretch on substrates

As depicted in Fig. 4, FEM simulations of a 2D plane strain finite element model show that when the flip-chip package is subject to a temperature change, e.g. $\Delta T < 0$, the singular stress fields at chip-substrate corners can be completely counteracted by a uniform uniaxial tensile stress p exerting on the substrate. This appendix derives the relation between p and ΔT.

Firstly, assume the chip and the substrate are separated and become freestanding. Both the chip and the substrate are subject to thermal loading ΔT but the substrate has to be uniaxially stretched to cancel its strain mismatch with the chip. Then if the chip and the substrate are put together, no singular stress will be developed around the bimaterial interface corner, as shown in the middle configuration of Fig. 4. Referring to the coordinate shown in Fig. 4, plane strain condition requires $\varepsilon_z = 0$.

In the chip

$$\varepsilon_z^{(c)} = \frac{\sigma_z}{E_c} - v_c\frac{\sigma_x}{E_c} - v_c\frac{\sigma_y}{E_c} + \alpha_c\Delta T = 0. \tag{B1}$$

No traction is applied to the chip, hence $\sigma_x = \sigma_y = 0$, solving Eq. (B1) gives

$$\sigma_z = -E_c\alpha_c\Delta T. \tag{B2}$$

Hence

$$\varepsilon_x^{(c)} = \frac{\sigma_x}{E_c} - v_c\frac{\sigma_y}{E_c} - v_c\frac{\sigma_z}{E_c} + \alpha_c\Delta T = (1+v_c)\alpha_c\Delta T. \tag{B3}$$

On the substrate, $\sigma_x = p$, $\sigma_y = 0$

Plane strain condition requires

$$\varepsilon_z^{(s)} = \frac{\sigma_z}{E_s} - v_s\frac{\sigma_x}{E_s} - v_s\frac{\sigma_y}{E_s} + \alpha_s\Delta T = 0, \tag{B4}$$

and σ_z can be expressed in terms of p

$$\sigma_z = v_s p - E_s\alpha_s\Delta T. \tag{B5}$$

Therefore

$$\varepsilon_x^{(s)} = \frac{\sigma_x}{E_s} - v_s\frac{\sigma_y}{E_s} - v_s\frac{\sigma_z}{E_s} + \alpha_s\Delta T = (1-v_s^2)\frac{p}{E_s} + (1+v_s)\alpha_s\Delta T. \tag{B6}$$

No mismatch between chip and substrate requires $\varepsilon_x^{(c)} = \varepsilon_x^{(s)}$. Solving the equation yields

$$p = \frac{E_s}{(1-v_s^2)}[(1+v_c)\alpha_c - (1+v_s)\alpha_s]\Delta T. \tag{B7}$$

If a 3D configuration is considered, an equivalent biaxial tensile stress p_{3D} can be derived following a similar approach:

$$p_{3D} = \frac{E_s}{(1-v_s)}(\alpha_c - \alpha_s)\Delta T. \tag{B8}$$

Table A1
Coefficients appearing in eigenfunctions given by Eqs. (A1), (A2), (A3), (A4).

	Mode 1				Mode 2			
	A_1	B_1	C_1	D_1	A_2	B_2	C_2	D_2
Si	0.5752	−0.8429	−2.2700	1.9937	0.9989	0.2841	−0.9955	0.8666
FR4	0.0010	−1.7404	−4.6075	0.7720	0.6337	−0.6262	−1.2579	−0.3421
Si	0.9937	0.3675	−0.6756	1.8257	0.9889	0.3764	−0.6915	1.8169
LTCC	0.1349	−1.9634	−8.5779	−0.5894	0.1623	−1.8439	−8.0551	−0.7089

References

[1] Atluri VP, Mahajan RV, Patel PR, Mallik D, Tang J, Wakharkar VS, et al. Critical aspects of high-performance microprocessor packaging. MRS Bull 2003;28(1):21–34.

[2] Reuss RH, Chalamala BR. Microelectronics packaging and integration. MRS Bull 2003;28(1):11–5.

[3] Tummala RR, Raj PM, Atmur S, Bansal S, Banerji S, Liu FH, et al. Fundamental limits of organic packages and boards and the need for novel ceramic boards for next generation electronic packaging. J Electroceram 2004;13(1–3):417–22.

[4] Frear DR, Thomas S. Emerging materials challenges in microelectronics packaging. MRS Bull 2003;28(1):68–74.

[5] Madenci E, Shkarayev S, Mahajan R. Potential failure sites in a flip-chip package with and without underfill. J Electron Packag 1998;120(4):336–41.

[6] Qian Z, Akisanya AR. An experimental investigation of failure initiation in bonded joints. Acta Mater 1998;46(14):4895–904.

[7] Chen L, Zhang Q, Wang GZ, Xie XM, Cheng ZN. The effects of underfill and its material models on thermomechanical behaviors of a flip chip package. IEEE Trans Adv Packag 2001;24(1):17–24.

[8] Fan XJ, Wang HB, Lim TB. Investigation of the underfill delamination and cracking in flip-chip modules under temperature cyclic loading. IEEE Trans Compon Packag Technol 2001;24(1):84–91.

[9] Gu Y, Nakamura T, Chen WT, Cotterell B. Interfacial delamination near solder bumps and UBM in flip-chip packages. J Electron Packag 2001;123(3):295–301.

[10] Choi WJ, Yeh ECC, Tu KN. Mean-time-to-failure study of flip chip solder joints on Cu/Ni(V)/Al thin-film under-bump-metallization. J Appl Phys 2003;94(9):5665–71.

[11] Mercado LL, Wieser H, Hauck T. Multichip package delamination and die fracture analysis. IEEE Trans Adv Packag 2003;26(2):152–9.

[12] Zhai CJ, Sidharth, Blish RC, Master RN. Investigation and minimization of underfill delamination in flip chip packages. IEEE Trans Device Mater Reliab 2004;4(1):86–91.

[13] Kwon WS, Yim MJ, Paik KW, Ham SJ, Lee SB. Thermal cycling reliability and delamination of anisotropic conductive adhesives flip chip on organic substrates with emphasis on the thermal deformation. J Electron Packag 2005;127(2):86–90.

[14] Wang GT, Merrill C, Zhao JH, Groothuis SK, Ho PS. Packaging effects on reliability of Cu/Low-k interconnects. IEEE Trans Device Mater Reliab 2003;3(4):119–28.

[15] Dundurs J. Discussion of a paper by D.B. Bogy. J Appl Mech 1969;36:650–2.

[16] Dempsey JP, Sinclair GB. Stress singularities in the plane elasticity of the composite wedge. J Elast 1979;9(4):373–91.

[17] Dempsey JP, Sinclair GB. On the singular behavior at the vertex of a bi-material wedge. J Elast 1981;11(3):317–27.

[18] Liu XH, Suo Z, Ma Q. Split singularities: stress field near the edge of a silicon die on a polymer substrate. Acta Mater 1998;47(1):67–76.

[19] Im S, Kim KS. An application of two-state M-integral for computing the intensity of the singular tip field for a generic wedge. J Mech Phys Solids 2000;48(1):129–51.

[20] Williams ML. Stress singularities resulting from various boundary conditions in angular corners of plates in extension. J Appl Mech 1952;19(4):526–8.

[21] Bogy DB. 2 edge-bonded elastic wedges of different materials and wedge angles under surface tractions. J Appl Mech 1971;38(2):377.

[22] Hein VL, Erdogan F. Stress singularities in a 2-material wedge. Int J Fract Mech 1971;7(3):317.

[23] Zhang Z, Suo Z. Split singularities and the competition between crack penetration and debond at a bimaterial interface. Int J Solids Struct 2007;44:4559–73.

[24] Hui CY, Ruina A. Why k-high-order singularities and small-scale yielding. Int J Fract 1995;72(2):97–102.

[25] Labossiere PEW, Dunn ML. Fracture initiation at three-dimensional bimaterial interface corners. J Mech Phys Solids 2001;49(3):609–34.

[26] Reedy ED. Connection between interface corner and interfacial fracture analyses of an adhesively-bonded butt joint. Int J Solids Struct 2000;37(17):2429–42.

[27] Dunn ML, Hui CY, Labossiere PEW, Lin YY. Small scale geometric and material features at geometric discontinuities and their role in fracture analysis. Int J Fract 2001;110(2):101–21.

[28] Labossiere PEW, Dunn ML, Cunningham SJ. Application of bimaterial interface corner failure mechanics to silicon/glass anodic bonds. J Mech Phys Solids 2002;50(3):405–33.

[29] Rice JR. Elastic fracture-mechanics concepts for interfacial cracks. J Appl Mech-Trans ASME 1988;55(1):98–103.

[30] Dunn ML, Cunningham SJ, Labossiere PEW. Initiation toughness of silicon/glass anodic bonds. Acta Mater 2000;48(3):735–44.

[31] Reedy ED, Guess TR. Nucleation and propagation of an edge crack in a uniformly cooled epoxy/glass bimaterial. Int J Solids Struct 2002;39(2):325–40.

[32] Zhang Z, Yoon J, Suo Z. Method to analyze dislocation injection from sharp features in strained silicon structures. Appl Phys Lett 2006;89:261912.

[33] Shin KC, Kim WS, Lee JJ. Application of stress intensity to design of anisotropic/isotropic bi-materials with a wedge. Int J Solids Struct 2007;44(24):7748–66.